Towards a Connected Sky: Performance of Beamforming with Down-tilted Antennas for Ground and UAV User Co-existence

Ramy Amer, *Student Member, IEEE,* Walid Saad, *Fellow, IEEE,* and Nicola Marchetti, *Senior Member, IEEE*

Abstract—Providing connectivity to aerial users (AUs) such as cellular-connected unmanned aerial vehicles (UAVs) is a key challenge for tomorrow's cellular systems. In this paper, the use of conjugate beamforming (CB) for simultaneous content delivery to an AU co-existing with multiple ground users (GUs) is investigated. In particular, a content delivery network of uniformly distributed massive multiple-input multiple-output (MIMO)-enabled ground base stations (BSs) serving both aerial and ground users through spatial multiplexing is considered. For this model, the successful content delivery probability (SCDP) is derived as a function of the system parameters. The effects of various system parameters such as antenna down-tilt angle, AU's altitude, number of scheduled users, and number of antennas on the achievable performance are then investigated. Results reveal that whenever the AU's altitude is below the BS height, the antennas' down-tilt angles yield an inherent tradeoff between the performance of the AU and the GUs. However, if the AU's altitude exceeds the BS height, down-tilting the BS antennas with a considerably large angle improves the performance of both the AU and the GUs.

Index Terms—Cellular-connected UAVs, conjugate beamforming.

I. INTRODUCTION

A tremendous increase in the use of unmanned aerial vehicles (UAVs) in a wide range of applications, ranging from delivery of goods to traffic control, is expected in the foreseeable future [1], [2]. To enable these applications, UAVs must communicate with one another and with ground devices. To enable such communications, it is imperative to connect UAVs, seen as aerial users (AUs), to the ubiquitous wireless cellular network. Such cellular-connected UAVs have recently attracted attention in cellular network research in both academia and industry [3]–[7] due to their ability to pervasively communicate. However, cellular networks have been designed to provide connectivity to ground users (GUs) rather than AUs [3]. For instance, cellular-connected UAV communication possesses substantially different characteristics that pose new technical challenges which include: dominance of line-of-sight (LoS) interference and reduced ground base stations (GBSs) antenna gain [3].

In this regard, the authors in [3] studied the feasibility of supporting drone operations using existing cellular infrastructure. Results revealed that the favorable propagation conditions that AUs enjoy due to their altitude is also one of their strongest limiting factors since they are susceptible to LoS interference. Meanwhile, the authors in [5] minimized the UAV's mission completion time by optimizing its trajectory while maintaining reliable communication with the GBSs. In [6], through system simulations, the authors evaluated the performance of the downlink of AUs when supported by either a traditional cellular network, or a massive multiple-input multiple-output (MIMO)-enabled network with zero-forcing beamforming (ZFBF). In [7], the authors showed that cooperative transmission significantly improves the coverage probability for high-altitude AUs. However, while the works in [3], [5], and [7] have analyzed the

performance of cellular-connected UAVs, their approaches can not be used to effectively improve the performance of AUs while enhancing spectral efficiency (SE) by spatial multiplexing. Also, although the work in [6] has proposed MIMO beamforming for an AU co-existing with GUs, this work provides no analytical characterization of the performance of AUs or the impact of the antennas' down-tilt angles.

The main contribution of this paper is a comprehensive analysis of cellular communications with AUs. In particular, we propose a MIMO *conjugate beamforming (CB)* approach that can improve the performance of cellular communication links for the AUs and effectively enhance the cellular system SE. We consider a network of one AU co-existing with multiple GUs that are being simultaneously served via massive MIMO-enabled GBSs. We introduce a novel analytical framework that can be leveraged to characterize the performance of the spatially multiplexed AU and GUs. Given the different channel characteristics and the corresponding precoding vectors among GUs and the AU, we first derive the gain of intended and interfering channels for both kind of users. We then analytically characterize the successful content delivery probability (SCDP) as a function of the system parameters. *To our best knowledge, this is the first work to perform a rigorous analysis of MIMO CB to simultaneously serve aerial and ground users.*

II. SYSTEM MODEL

Consider a cellular network composed of massive MIMO-enabled base stations (BSs) b_i distributed according to a homogeneous Poisson point process (PPP) Φ of intensity λ, where $\Phi = \{b_i \in \mathbb{R}^2, \forall i \in \mathbb{N}^+\}$. A three-sectored cell is associated with each BS, with each sector spanning an angular interval of $120\,°$. Each sector has a large antenna array of M antennas each of which has a horizontal constant beamwidth of $120\,°$, and vertical beamwidth θ_B. CB is employed to simultaneously serve a selected set $\mathcal{K}$ of K users. These K users are viewed as an AU that is scheduled with a set $\mathcal{K}_G$ of $K-1$ GUs, as done in [6]. This assumption is in line with the fact that the number of current GUs is much larger than the number of AUs. We assume that the GUs are located according to some independent stationary point process. BSs are deployed at the same height h_{BS} while AUs and GUs are at altitudes h_d and h_g, respectively, where $h_d \gg h_g$. Given the symmetry of the problem, we consider the performance of the typical ground and aerial users located at $(0, 0, h_g)$, and $(0, 0, h_d)$, respectively. We also refer to the serving BS as *tagged BS*, which is the nearest BS to the origin $(0, 0) \in \mathbb{R}^2$, with d_{ig} and d_{id} being the distances from the GBS to the typical GU and AU, respectively.

For GUs, we consider independently and identically distributed (i.i.d.) quasi-static Rayleigh fading channels. The channel vector between the M antennas of tagged BS i and GU k is $\sqrt{\beta_{ik}}\boldsymbol{h}_{ik}$, where $\boldsymbol{h}_{ik} \sim \mathcal{CN}(\boldsymbol{0}, \sigma^2 \boldsymbol{I}_M)$ for $k \in \mathcal{K}_G$. σ^2 is the channel variance between each single antenna and user k, and $\boldsymbol{I}_M$ is the $M \times M$ identity matrix. $\beta_{ik} = d_{ig}^{-\alpha}$ defines the large-scale channel fading. We also assume that the GU channels are dominated by non-line-of-sight (NLoS) transmission. For the AU, we assume a wireless channel that is characterized by both large-scale and small-scale fading. For the large-scale fading, the channel between BS i and the AU includes LoS and NLoS components, which are

considered separately along with their probabilities of occurrence [8]. For small-scale fading, we adopt a Nakagami-m_v model for the channel between each single antenna and the AU, as done in [7]–[9], with the following probability distribution function (PDF): $f_{\Omega_v}(\omega, \eta) = \frac{2(\frac{m_v}{\eta})^{m_v}\omega^{2m_v-1}}{\Gamma(m_v)}\exp\left(-\frac{m_v}{\eta}\omega^2\right)$, where $v \in \{l, n\}$, m_l and m_n are the fading parameters for the LoS and NLoS links, respectively, with $m_l > m_n$, and η is a controlling spread parameter. When $m_v = \eta = 1$, Rayleigh fading is recovered with an exponentially distributed instantaneous power, which is the case for GUs or AUs with no LoS communication. For Nakagami channels, we assume that the phase θ_{ng} is uniformly distributed in $[0, 2\pi]$, i.e., $\theta_{ng} \sim \mathcal{U}(0, 2\pi)$. Given that $\omega \sim$ Nakagami(m_v, η), it directly follows that the channel gain $\omega^2 \sim \Gamma(m_v, \frac{\eta}{m_v})$.

3D blockage is characterized by the fraction a of the total land area occupied by buildings, the mean number of buildings being ν per km^2, and the buildings' height modeled by a Rayleigh PDF with a scale parameter c. Hence, the probability of LoS when served from BS i, at a horizontal-distance r_i from the typical AU, is given as [3]: $\mathbb{P}_l(r_i) = \prod_{n=0}^{p}\left[1-\exp\left(-\frac{\left(h_{\text{BS}}+\frac{h(n+0.5)}{p+1}\right)^2}{2c^2}\right)\right]$, where $h = h_d - h_{\text{BS}}$ and $p = \lfloor\frac{r_i\sqrt{a\nu}}{1000} - 1\rfloor$. In our model, we assume that the AUs are deployed in an urban environments, where a and ν take relatively large values. Therefore, the large-scale channel fading for the AU is given by $d_{id}^{-\alpha_v}$, where $v \in \{l, n\}$, α_l and α_n are the path loss exponents for LoS and NLoS links, respectively, with $\alpha_l < \alpha_n$.

For a general user $k \in \mathcal{K}$ at altitude $h_k \in \{h_d, h_g\}$, the antenna directivity gain can be written similar to [3] as $G(r_i) = G_m$, for $r_i \in \mathcal{S}_{bs}$, and G_s, for $r_i \notin \mathcal{S}_{bs}$, where r_i is the horizontal-distance to the BS, $\mathcal{S}_{bs}$ is formed by all the distances r_i satisfying $h_{\text{BS}} - r_i\tan(\theta_t + \frac{\theta_B}{2}) < h_k < h_{\text{BS}} - r_i\tan(\theta_t - \frac{\theta_B}{2})$, and θ_t and θ_B denote respectively the antenna down-tilt and beamwidth angles. Therefore, the antenna gain plus path loss will be

$$\zeta_v(r_i) = A_v G(r_i) d_i^{-\alpha_v} = A_v G(r_i)\left(r_i^2 + (h_k - h_{\text{BS}})^2\right)^{-\alpha_v/2},$$

where $d_i \in \{d_{ig}, d_{id}\}$, and A_l and A_n are the path loss constants at a reference distance $d_i = 1\,\text{m}$ for LoS and NLoS, respectively. For the typical GU, $d_i = d_{ig}$, $h_k = h_g$ and, by NLoS assumption, $v = n$. Note that, since one AU is simultaneously scheduled with $K - 1$ GUs, the K scheduled users encounter independent small-scale fading. Also, for the $K - 1$ GUs, the small-scale fading is i.i.d. Moreover, for the AU, the impact of the channel spatial correlation can be significantly reduced using effective MIMO antenna design techniques, e.g., using antenna arrays whose elements have orthogonal polarizations or patterns [10]. Therefore, for analytical tractability, we ignore such spatial correlation.

III. CONTENT DELIVERY ANALYSIS

We assume that perfect channel state information (CSI) is available at the tagged BS. Linear precoding in terms of CB creates a $K \times 1$ transmission vector $\boldsymbol{s}'$ for M antennas by multiplying the original data vector $\boldsymbol{s}$ by a precoding matrix $\boldsymbol{W}$: $\boldsymbol{s}' = \boldsymbol{W}\cdot\boldsymbol{s}$, where $[\boldsymbol{W}]_{M\times K}$ consists of the beamforming weights. Let $\boldsymbol{H}$ be the $M \times K$ channel matrix between M antennas of the tagged BS i and its K scheduled users, written as $\boldsymbol{H}_i = \left[\boldsymbol{h}_{i1}\ldots\boldsymbol{h}_{ik}\ldots\boldsymbol{h}_{iK}\right]$, where $\boldsymbol{H}_i \in \mathbb{C}^{M\times K}$, and $\boldsymbol{h}_{ik} \in \mathbb{C}^{M\times 1}$. For CB, tagged BS i creates a precoding matrix $\boldsymbol{W}_i = \left[\boldsymbol{w}_{i1}\ldots\boldsymbol{w}_{ik}\ldots\boldsymbol{w}_{iK}\right]$, with $\boldsymbol{w}_{ik} = \frac{\boldsymbol{h}_{ik}^H}{\|\boldsymbol{h}_{ik}\|}$, where each beam is normalized to ensure equal power assignment [11]. Moreover, let $\boldsymbol{f}_{jk}$ be the interfering channel between interfering BS j and typical user k. Neglecting thermal noise, the received signal at scheduled user k, denoted as y_{ik}, is given by

$$P(r_i)\boldsymbol{h}_{ik}\boldsymbol{w}_{ik}s_{ik} + \sum_{\kappa\in\mathcal{K}_G}P(r_i)\boldsymbol{h}_{ik}\boldsymbol{w}_{i\kappa}s_{i\kappa} + \sum_{j\in\Phi^o}\sum_{l=1}^{K}P(u_j)\boldsymbol{f}_{jk}\boldsymbol{w}_{jl}s_{jl},$$

TABLE I
CHANNEL GAINS FOR INTENDED AND INTERFERING LINKS.

No	Precoding for channel	Traverse through channel	Seen by	Intended	Channel gain
1	$\mathcal{CN}(0, \frac{\sigma^2}{2})$	$\mathcal{CN}(0, \frac{\sigma^2}{2})$	GU	Yes	$\Gamma(M, \sigma^2)$
2	Nakagami(m_v, η)	Nakagami(m_v, η)	AU	Yes	$\Gamma(m_v M, \frac{\eta}{m_v})$
3	$\mathcal{CN}(0, \frac{\sigma^2}{2})$	$\mathcal{CN}(0, \frac{\sigma^2}{2})$	GU	No	$\Gamma(1, \sigma^2)$
4	$\mathcal{CN}(0, \frac{\sigma^2}{2})$	Nakagami(m_v, η)	AU	No	$\Gamma(1, \eta)$
5	Nakagami(m_v, η)	$\mathcal{CN}(0, \frac{\sigma^2}{2})$	GU	No	$\Gamma(1, \sigma^2)$
6	Nakagami(m_v, η)	Nakagami(m_v, η)	AU	No	$\Gamma(1, \eta)$

where $\Phi^o = \Phi \setminus \{i\}$. The first term in the above equation represents the desired signal from tagged BS i with $P(r_i) = \sqrt{\frac{P_t}{K}}\zeta_v(r_i)^{0.5}$ representing the received power and P_t denoting the BS transmission power. The second and third terms represent the intra- and inter-cell interference, denotes as I_{in} and I_{out}, respectively. The information signal intended for user k is denoted by a complex scalar s_{ik} with unit average power, i.e., $\mathbb{E}[|s_{ik}|^2] = 1$.

Since we assume both LoS and NLoS communications for the AU, with corresponding small-scale fading, we need to distinguish between the two communication paradigms. For the NLoS case, all the K users experience Rayleigh small-scale fading. For LoS communication, however, only the AU experiences Nakagami-m_l small-scale fading, where $m_l > 1$. We hence start by characterizing the gain of intended and interfering channels in Table I.

The second and third columns in Table I list the marginal channel distributions, i.e., the channel from each single antenna to its intended receiver. We also use interfering BSs to refer to either intra- or inter-cell BS. The first row in Table I represents the intended channel gain for GUs. It is shown that the equivalent channel gain from tagged BS to its associated GU follows $\Gamma(M, \sigma^2)$ [11]. Similarly, the second row represents the intended channel gain for the AU, which is the sum of M independent random variables (RVs), each of which follows $\Gamma(m_v, \frac{\eta}{m_v})$. Hence, its intended channel gain follows $\Gamma(m_v M, \frac{\eta}{m_v})$. The third row stands for the interference power caused by transmission of a single beam from an interfering BS to its associated GU when seen by the typical GU, which follows $\Gamma(1, \sigma^2)$ [11]. The fourth (fifth) row describes cases in which a single beam from an interfering BS to its associated GU (AU) is transmitted and seen by the typical AU (GU). Similarly, the sixth row describes cases in which a single beam from an interfering BS to its associated AU is transmitted and seen by the typical AU. Next, we derive the channel gain for the fourth case, whereas the fifth and sixth cases follow in the same way and are omitted due to space limitations.

Theorem 1. *Under the massive MIMO assumption, whenever a single beam from an interfering BS is received by the typical AU then, the interference channel gain will be given by $\Gamma(1, \eta)$.*

Proof. We write the interfering channel coefficient as

$$h_j = \boldsymbol{w}_{j\kappa}\boldsymbol{f}_{jk} = \frac{\boldsymbol{h}_{j\kappa}^H\boldsymbol{f}_{jk}}{\|\boldsymbol{h}_{j\kappa}\|} \triangleq \frac{\sum_{o=1}^{M}X_o\times Y_o}{\sqrt{\sum_{q=1}^{M}Z_q}} \qquad (1)$$

$$\overset{(a)}{\triangleq} \frac{\sum_{o=1}^{M}X_o\times Y_o}{\sqrt{W}} \overset{(b)}{\triangleq} \frac{\sum_{o=1}^{M}X_o\times Y_o}{Q}, \qquad (2)$$

where $X_o \sim \mathcal{CN}(0, \frac{\sigma^2}{2})$, $Y_o \sim$ Nakagami(m_v, η), $Z_q \sim \exp(\frac{1}{\sigma^2})$, $W \sim \Gamma(M, \frac{1}{\sigma^2})$, and $Q \sim$ Nakagami$(M, \frac{M}{\sigma^2})$; (a) follows since W is a sum of M i.i.d. exponential RVs, hence it follows $\Gamma(M, \frac{1}{\sigma^2})$. (b) follows since Q equals the square root of the RV $W \sim \Gamma(M, \frac{1}{\sigma^2})$, hence Q follows Nakagami$(M, \frac{M}{\sigma^2})$. Denoting the numerator of h_j as z, and writing z as sum of real and imaginary RVs:

$$\text{Re}(z) \triangleq \sum_{o=1}^{M}\left(\underbrace{X_o\cos(\theta_{ng_o}) - X_o\sin(\theta_{ng_o})}_{\text{RV\#1}}\right)\cdot\underbrace{Y_o}_{\text{RV\#2}}, \qquad (3)$$
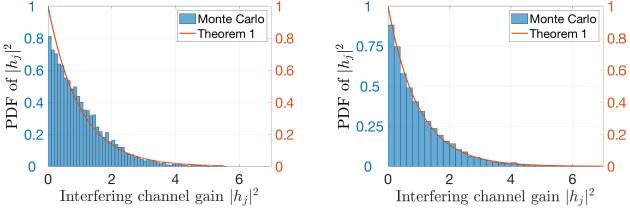
(a) Number of antennas $M = 4$ (b) Number of antennas $M = 32$

Fig. 1. PDF of the interfering channel power.

(a) AU altitude $h_d = 90\,\mathrm{m}$ (b) $\vartheta = 5\,\mathrm{dB}$, $\lambda = 50\,\mathrm{km}^{-2}$

Fig. 2. Effect of SIR threshold and AU altitude ($h_{\mathrm{BS}} = 30\,\mathrm{m}$).

(a) AU altitude $h_d = 30\,\mathrm{m}$ (b) AU altitude $h_d = 80\,\mathrm{m}$

Fig. 3. Effect of antenna down-tilt angle.

where, by assumption, $\theta_{ng_o} \sim \mathcal{U}(0, 2\pi)$. We hence have a sum of M i.i.d. RVs, each of which is the product of two independent RVs whose means and variances are $\{\mu_1, \mu_2\}$ and $\{\sigma_1^2, \sigma_2^2\}$, respectively. It can easily be shown that $\mu_1 = 0$ and $\sigma_1^2 = \frac{\sigma^2}{2}$. For large M, using the central limit theorem (CLT), we approximate the PDF of $\mathrm{Re}(z)$ to $\mathcal{N}(\mu_{12}, \sigma_{12}^2)$, whose mean and variance are respectively $\mu_{12} = \mu_1 \mu_2 = 0$, and $\sigma_{12}^2 = \sigma_1^2 \sigma_2^2 + \sigma_1^2 \mu_2^2 + \mu_1^2 \sigma_2^2 \stackrel{(a)}{=} \frac{\sigma^2}{2}\eta\Big(1 - \frac{1}{m_v}\Big(\frac{\Gamma(m_v+0.5)}{\Gamma(m_v)}\Big)^2\Big) + \frac{\sigma^2}{2}\Big(\frac{\Gamma(m_v+0.5)}{\Gamma(m_v)}\Big(\frac{\eta}{m_v}\Big)^{0.5}\Big)^2 = \frac{\sigma^2 \eta}{2}$, where (a) follows from the mean and variance formulas for Nakagami(m_v, η). For the dominator of (2), we use the Stirling approximation to approximate the PDF of Q by $f_\Omega(\omega, M, M/\sigma^2) = \frac{1}{\omega}\Big(\frac{\omega^2}{\frac{M}{\sigma^2}e^{\frac{\omega^2}{M/\sigma^2}-1}}\Big)^M$.

The fraction raised to the M-th power is smaller than one, and the integral is one (since it is a PDF). In fact, the factor raised to the M-th power is one only when $\omega = \frac{\sqrt{M}}{\sigma}$. Hence, for large M, from the CLT, $\mathrm{Re}(h_j) \sim \frac{\mathcal{N}\left(0, \frac{\sigma^2 \eta}{2M}\right)}{\frac{\sigma}{\sqrt{M}}} \triangleq \mathcal{N}(0, \frac{\eta}{2})$. Similarly, $\mathrm{Im}(h_j) \sim \mathcal{N}(0, \frac{\eta}{2})$. Hence, the channel gain $|h_j|^2 = \left(\sqrt{\mathrm{Re}\{h_j\}^2 + \mathrm{Im}\{h_j\}^2}\right)^2 \sim \Gamma(1, \eta)$. This completes the proof. $\square$

Next, we derive the SCDP for the AU, which is defined as the probability of obtaining a requested content with signal-to-interference-ratio (SIR) higher than a target SIR ϑ. The same methodology can be applied to obtain that for GUs, but the details are omitted due to space constraints. We next index the AU as $k = 1$. Let $h_{iK} = \sum_{\kappa \in \mathcal{K}_G} |\boldsymbol{w}_{i\kappa} \boldsymbol{f}_{i1}|^2$ denote the intra-cell interference power. From Theorem 1, $|\boldsymbol{w}_{i\kappa} \boldsymbol{f}_{i1}|^2 \sim \Gamma(1, \eta)$. Neglecting the spatial correlation, we have h_{iK} representing sum of $K - 1$ Gamma RVs, which yields $h_{iK} \sim \Gamma(K-1, \eta)$. Similarly, the inter-cell interference power $h_{jK} = \sum_{l=1}^K |\boldsymbol{w}_{il} \boldsymbol{f}_{j1}|^2 \sim \Gamma(K, \eta)$. Finally, according to the void probability of PPPs [12], the PDF of the horizontal-distance r to the *tagged BS* is $f_R(r) = 2\pi \lambda r e^{-\pi \lambda r^2}$.

Theorem 2. *The unconditional SCDP for the AU is given by*

$$\mathbb{P}_c = \mathbb{P}\big(\mathrm{SIR} > \vartheta\big) = \int_{r=0}^\infty \Big[\mathbb{P}_{c|r}^l \mathbb{P}_l(r) + \mathbb{P}_{c|r}^n \mathbb{P}_n(r)\Big] f_R(r)\, dr, \quad (4)$$

where $\mathbb{P}_{c|r}^v = \|e^{\boldsymbol{T}_{M_v}}\|_1$, $\|.\|_1$ *denotes the induced* ℓ_1 *norm, and* $\boldsymbol{T}_{M_v}$ *is the lower triangular Toeplitz matrix of size* $M_v \times M_v$, $M_v = Mm_v$, *whose non-zero entries for row i and column j are* $t_{i-j} = \frac{(-s_v)^{i-j}}{(i-j)!}\varpi^{(i-j)}(s_v)$; $s_v = \frac{\vartheta K m_v}{\eta P_t \zeta_v(r)}$, $\varpi(s_v) = -(K-1)\log(1 + s_v \eta P_v(r)^2) - 2\pi \lambda \int_{\nu=r}^\infty \big(1 - \mathbb{P}_l(\nu)\delta_l(\nu, s_v) - \mathbb{P}_n(\nu)\delta_n(\nu, s_v)\big)\nu\, d\nu$, *and* $\varpi^{(k)(s_v)} = \frac{d^k}{ds_v^k}\varpi(s_v)$; $\delta_l(\nu, s_v) = \big(1 + s_v \eta P_l(\nu)^2\big)^{-K}$, *and* $\delta_n(\nu, s_v) = \big(1 + s_v \eta P_n(\nu)^2\big)^{-K}$.

Proof. Please see Appendix A. $\square$

Remark 1. The main merit of this representation, i.e., $\mathbb{P}_{c|r}^v = \|e^{\boldsymbol{T}_{M_v}}\|_1$, is that it leads to valuable system insights. For example, the impact of the shape parameter $M_v = Mm_v$ on the intended channel gain $h_{iK} \sim \Gamma(Mm_v, \eta/m_v)$, which is typically related to the antenna size and the Nakagami fading parameter m_v, is
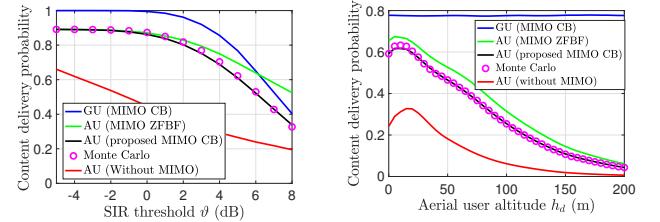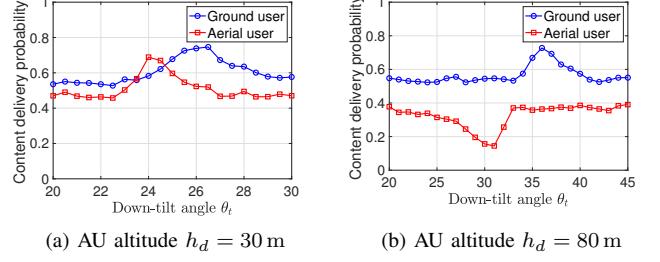
clearly illustrated by this finite sum representation (5). Although it is not tractable to obtain closed-form expressions for t_k (the entries populating $\boldsymbol{T}_{M_v}$), special cases of interest, e.g., LoS or NLoS communications, can lead to closed-form expressions, following [13].

Remark 2. When $K = 1$, only the AU is scheduled, i.e., maximal ratio transmission (MRT) beamforming. For MRT, the interfering channel gain is $\Gamma(1, \eta)$. Interestingly, this interfering channel gain is reduced as opposed to the typical Nakagami channel gain $\Gamma\big(m_l, \frac{\eta}{m_l}\big)$ when there is neither precoding nor MIMO transmission.

IV. NUMERICAL RESULTS

For our simulations, we consider a network having the following parameters, unless otherwise specified. The number of antennas per sector is set to $M = 32$. We also set $K = 4$, $\lambda = 1\,\mathrm{km}^{-2}$, $h_{\mathrm{BS}} = 55\,\mathrm{m}$, $h_g = 1\,\mathrm{m}$, $\alpha_l = 2.09$, $\alpha_n = 3.75$, $a = 0.6$, $\nu = 500\,\mathrm{km}^{-2}$, $c = 25$, $\vartheta = 10\,\mathrm{dB}$, $A_l = -41.1\,\mathrm{dB}$, $A_n = -32.9\,\mathrm{dB}$, $G_m = 10\,\mathrm{dB}$, $G_s = -3.01\,\mathrm{dB}$, $m_n = 1$, $m_l = 3$, $\eta = 1$, $\sigma^2 = 1$, $\theta_B = 45^\circ$, $\theta_t = 30^\circ$.

In Fig. 1, we verify the accuracy of the obtained PDF of interfering channel gain $|h_j|^2$ (Table I: row 4) in Theorem 1. The figure shows that the derived PDF is quite accurate when M is sufficiently large as in Fig. 1(b), while for small M in Fig. 1(a), it still provides a reasonable approximation.

Fig. 2 compares the SCDP of AUs with and without MIMO beamforming to GUs. Fig. 2(a) plots the SCDP as a function of the SIR threshold ϑ for the AU and the GUs. Clearly, the achievable performance of GUs considerably outperforms that of an AU. This is because GUs have a superior propagation environment, driven by the down-tilted BS antennas in the desired signal side, and the NLoS interfering links. However, Fig. 2 also shows that the SCDP for the AU served by MIMO CB significantly outperforms that of the AU served by single-antenna GBSs. Moreover, although the ZFBF technique outperforms our proposed CB approach, the low complexity of CB and its associated performance gain over traditional single-antenna GBSs make it a good candidate to serve AUs. Fig. 2(b) shows the effect of AU altitude on the AU performance, with that of GUs plotted for comparison. For all transmission schemes, the AU SCDP gradually increases with h_d up to a maximum value due to the larger LoS probability, before it decreases again due to the stronger LoS interference and higher large scale fading.

Fig. 3 illustrates the effect of the down-tilt angle θ_t on the performance of both the AU and the GUs, for different AU altitudes.
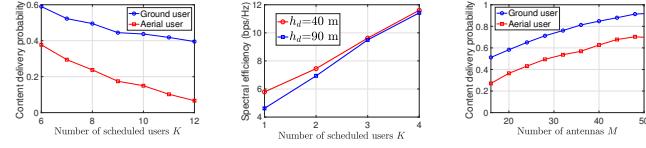
(a) Number of antennas $M = 32$ (b) Number of antennas $M = 32$ (c) Number of users $K = 4$

Fig. 4. Effect of the number of antennas and the number of scheduled users.

As illustrated in Fig. 3(a), for $h_d < h_{\text{BS}}$, the performance of the AU is maximized at certain θ_t, and beyond that it starts to degrade. However, for GUs, their performance is maximized at a higher θ_t. Hence, adjusting the antennas' down-tilt angle yields a tradeoff between the performance of AUs and GUs owing to the difference in their altitudes. For $h_d > h_{\text{BS}}$ in Fig. 3(b), the SCDP of the AU first decreases with θ_t to a minimum value, and then it increases again. This finding can be explained as follows: when θ_t is small, an AU at an altitude $h_d > h_{\text{BS}}$ can be served from the main lobe of tagged BS while also experiencing high interference from the main lobe of other interfering BSs. Gradually, as θ_t increases, the worst performance is observed when the AU is no longer served from the main lobe of tagged BS antennas while still experiencing high interference from the main lobe of other interfering BSs. Finally, for very large θ_t, both intended and interfering signals stem from the side-lobes, and hence the performance is improved again. In Fig. 4, we show the prominent effect of the number of scheduled users K and the number of antennas M on the network performance. Fig. 4(a) shows that the SCDP monotonically decreases for both AU and GU as K increases due to the effect of stronger interference. However, it is noticeable that increasing K highly degrades the AU performance compared to that of GUs. This stems from the fact that AUs are more sensitive to interference, which often exhibits LoS component. In Fig. 4(b), we show the system spectral efficiency (SE) versus the number of scheduled users K. In this figure, $K = 1$ means that only the AU is scheduled. Evidently, the system SE increases as K increases, which proves that spatially multiplexing one AU with the GUs significantly improves the system SE. Fig. 4(c) shows that increasing the number of antennas M improves the SCDP for both users with nearly the same rate.

V. Conclusion

In this paper, we have proposed a novel CB framework for spatially multiplexing AUs and GUs. In order to analytically express the SCDP, we have derived the gain of intended and interfering channels. We have shown that exploiting CB from massive MIMO-enabled BSs to spatially multiplex an AU and GUs substantially improves the performance of the AU, in terms of SCDP. We have then shown that the down-tilt of the BS antennas can lead to a tradeoff between the performance of AUs and GUs only if the AU's altitude is below the BS height. Simulation results have shown the various properties of cellular communications when AUs and GUs co-exist.

Appendix

The SCDP is defined as the probability of downloading content with a received SIR higher than a target threshold ϑ, i.e.,

$$\mathbb{P}_{\text{c}|r}^v = \mathbb{P}\Big(\frac{\frac{P_t}{K}\zeta_v(r)\big|\boldsymbol{w}_{i1}\boldsymbol{h}_{i1}\big|^2}{I} > \vartheta\Big) = \mathbb{P}\Big(\big|\boldsymbol{w}_{i1}\boldsymbol{h}_{i1}\big|^2 > \frac{\vartheta K}{P_t\zeta_v(r)}I\Big)$$

$$\overset{(a)}{=} \mathbb{E}_I\Big[\sum_{i=0}^{M_v-1}\frac{s_v^i}{i!}I^i e^{-s_v I}\Big] \overset{(b)}{=} \sum_{i=0}^{M_v-1}\frac{(-s_v)^i}{i!}\mathcal{L}_{I|r}^{(i)}(s_v), \quad (5)$$

where $I = I_{\text{in}} + I_{\text{out}}$, (a) follows from $|\boldsymbol{w}_{i1}\boldsymbol{h}_{i1}|^2 \sim \Gamma(M_v, \frac{\eta}{m_v})$, and (b) follows from the Laplace transform of interference, along

with the assumption of independence between the intra- and inter-cell interference. Next, we derive the Laplace transform of interference $\mathcal{L}_{I|r}(s_v)$ from:

$$= \mathbb{E}_I\Big[e^{-s_v I}\Big] = \mathbb{E}_{h_{iK}}e^{-s_v h_{iK}P(r)^2}\mathbb{E}_\Phi\prod_{j\in\Phi^o}\mathbb{E}_{h_{jK}}e^{-s_v h_{jK}P(u_j)^2}$$

$$\overset{(a)}{=} \Big(1 + s_v\eta P_v(r)^2\Big)^{-(K-1)}e^{-2\pi\lambda\mathbb{E}_{h_{jK}}\int_{\nu=r}^\infty\big(1-\exp(-s_v h_{jK}P(\nu)^2)\big)\nu d\nu}$$

$$\overset{(b)}{=} e^{-(K-1)\log(1+s_v\eta P_v(r)^2)}e^{-2\pi\lambda\mathbb{E}_{h_{jK}}\int_{\nu=r}^\infty\big(1-\exp(-s_v h_{jK}P(\nu)^2)\big)\nu d\nu}$$

$$\overset{(c)}{=} e^{-(K-1)\log(1+s_v\eta P_v(r)^2)}\times$$

$$e^{-2\pi\lambda\int_{\nu=r}^\infty\big(1-\mathbb{P}_l(\nu)\delta_l(\nu,s_v)-\mathbb{P}_n(\nu)\delta_n(\nu,s_v)\big)\nu d\nu} = e^{\varpi(s_v)},$$

where (a) follows from $h_{iK} \sim \Gamma(K-1, \eta)$ and the probability generating functional (PGFL) of PPP Φ [12]. (b) follows from the fact that $x = e^{\log(x)}$, and (c) follows since $h_{jK} \sim \Gamma(K, \eta)$. In [13], it is proved that $\sum_{i=0}^{M_v-1}\frac{(-s_v)^i}{i!}\mathcal{L}_{I|r}^{(i)}(s_v) = \sum_{i=0}^{M_v-1}p_i$, with $p_i = \frac{(-s_v)^i}{i!}\mathcal{L}_{I|r}^{(i)}(s_v)$ computed from the recursive relation: $p_i = \sum_{l=0}^{i-1}\frac{i-l}{i}p_l t_{i-l}$, where $t_k = \frac{(-s_v)^k}{k!}\varpi^{(k)}(s_v)$. After some algebraic manipulation, $\mathbb{P}_{\text{c}|r}^v$ can be expressed in a compact form $\mathbb{P}_{\text{c}|r}^v = \|e^{\boldsymbol{T}_{M_v}}\|_1$ as in [13]. In summary, we first derive the conditional log-Laplace transform $\varpi(s_v)$ of the aggregate interference. Then, we calculate the n-th derivative of $\varpi(s_v)$ to populate the entries t_n of the lower triangular Toeplitz matrix $\boldsymbol{T}_{M_v}$.

References

[1] M. Mozaffari, W. Saad, M. Bennis, Y. Nam, and M. Debbah, "A tutorial on UAVs for wireless networks: Applications, challenges, and open problems," *IEEE Communications Surveys Tutorials*, pp. 1–1, 2019.
[2] M. Mozaffari, W. Saad, M. Bennis, and M. Debbah, "Unmanned aerial vehicle with underlaid device-to-device communications: Performance and tradeoffs," *IEEE Transactions on Wireless Communications*, vol. 15, no. 6, pp. 3949–3963, June 2016.
[3] M. M. Azari, F. Rosas, A. Chiumento, and S. Pollin, "Coexistence of terrestrial and aerial users in cellular networks," in *Proc. of IEEE Globecom Workshops (GC Wkshps)*, Singapore, Dec 2017, pp. 1–6.
[4] X. Lin, V. Yajnanarayana, S. D. Muruganathan, S. Gao, H. Asplund, H.-L. Maattanen, M. Bergstrom, S. Euler, and Y.-P. E. Wang, "The sky is not the limit: LTE for unmanned aerial vehicles," *IEEE Communications Magazine*, vol. 56, no. 4, pp. 204–210, April 2018.
[5] S. Zhang, Y. Zeng, and R. Zhang, "Cellular-enabled UAV communication: A connectivity-constrained trajectory optimization perspective," *IEEE Transactions on Communications*, vol. 67, no. 3, pp. 2580–2604, March 2019.
[6] G. Geraci, A. Garcia-Rodriguez, L. G. Giordano, D. López-Pérez, and E. Björnson, "Understanding UAV cellular communications: From existing networks to massive MIMO," *IEEE Access*, vol. 6, pp. 67 853–67 865, 2018.
[7] R. Amer, W. Saad, H. ElSawy, M. Butt, and N. Marchetti, "Caching to the sky: Performance analysis of cache-assisted CoMP for cellular-connected UAVs," in *Proc. of the IEEE Wireless Communications and Networking Conference (WCNC)*, Marrakech, Morocco, April. 2019.
[8] B. Galkin, J. Kibilda, and L. Da Silva, "A stochastic model for UAV networks positioned above demand hotspots in urban environments," *IEEE Transactions on Vehicular Technology*, pp. 1–1, 2019.
[9] V. V. Chetlur and H. S. Dhillon, "Downlink coverage analysis for a finite 3-D wireless network of unmanned aerial vehicles," *IEEE Transactions on Communications*, vol. 65, no. 10, pp. 4543–4558, Oct 2017.
[10] R. Bhagavatula, R. W. Heath Jr, and K. Linehan, "Performance evaluation of MIMO base station antenna designs," *Antenna Systems and Technology Magazine*, vol. 11, no. 6, pp. 14–17, 2008.
[11] K. Hosseini, W. Yu, and R. S. Adve, "Large-scale MIMO versus network MIMO for multicell interference mitigation," *IEEE Journal of Selected Topics in Signal Processing*, vol. 8, no. 5, pp. 930–941, Oct 2014.
[12] M. Haenggi, *Stochastic geometry for wireless networks*. Cambridge University Press, 2012.
[13] X. Yu, C. Li, J. Zhang, M. Haenggi, and K. B. Letaief, "A unified framework for the tractable analysis of multi-antenna wireless networks," *IEEE Transactions on Wireless Communications*, vol. 17, no. 12, pp. 7965–7980, Dec 2018.